IEEE Access
Multidisciplinary | Rapid Review | Open Access Journal

Received October 3, 2019, accepted November 15, 2019, date of publication November 25, 2019,
date of current version December 23, 2019.

Digital Object Identifier 10.1109/ACCESS.2019.2955515

Stochastic Multi-Objective Optimized Dispatch of Combined Cooling, Heating, and Power Microgrids Based on Hybrid Evolutionary Optimization Algorithm

BIFEI TAN AND HAOYONG CHEN, (Senior Member, IEEE)
School of Electric Power Engineering, South China University of Technology, Guangzhou 510641, China

Corresponding author: Haoyong Chen (eehychen@scut.edu.cn)

This work was supported in part by the National Natural Science Foundation of China under Grant 51937005, and in part by the National Key Research and Development Program of China under Grant 2016YFB0900100.

ABSTRACT The penetration of distributed power sources has been increasing with the continuous promotion of clean renewable energy sources. This paper seeks to improve the utilization rate of clean energy and reduce the cost of microgrid operation by first establishing a double-layer wind power prediction error model based on a comprehensive consideration of the time-of-use price and the operating characteristics of different types of clean energy sources, such as wind power, photovoltaic power, thermal power, and transmission tie lines. A combined cooling, heating, and power microgrid collaborative optimization model that considers wind power forecast uncertainty is established with the goal of minimizing economic cost, environmental cost, and degree of power-generation unit output asynchrony of the microgrid. The established multi-objective optimization model is solved using an improved intelligent optimization algorithm that combines the non-dominated sorting genetic algorithm (NSGA) with co-evolution theory and the beetle antennae search algorithm. This algorithm employs a variety of groups in the NSGA to help with correcting the approximations of group members through competition and cooperation. Therefore, the proposed algorithm can combine the excellent convergence of the NSGA and the powerful searching ability of co-evolutionary algorithms. Finally, a practical microgrid system in Northwest China is simulated as a case study, and the performance of the proposed algorithm is compared with that of the conventional NSGA. The simulation results demonstrate the superiority of the global search performance and the rapid convergence performance of the proposed hybrid algorithm.

INDEX TERMS Microgrid, cooperative co-evolution theory, beta function, wind power forecast, CCHP, non-dominated sorting-based algorithm-II, Pareto optimality, beetle antennae search.

NOMENCLATURE

ABBREVIATION

CCHP	combined cooling, heating, and power
MG	microgrid
NSGA	non-dominated sorting-based algorithm
PV	photovoltaic
WT	wind turbine
AGC	automatic gain control
PSO	particle swarm optimization
GT	diesel engine
FC	fuel cell
AH	waste heat
HX	heat exchanger
AC	absorption chiller
EC	electric chiller
T	scheduling period
Y	total compensation due to inaccuracy

PARAMETERS

$h_{\mathrm{wt},i}(t)/u_{\mathrm{wt},i}(t)$	actual/predicted normalized outputs of wind turbine i at time t
$P_{\mathrm{wt},i}(t)$/ actual / predicted outputs of wind turbine i at t	

The associate editor coordinating the review of this manuscript and approving it for publication was Amedeo Andreotti.

$k_{\mathrm{WT},j}$	cost coefficient of jth wind turbine
$P_{\mathrm{theory-max,wt}}$	theoretical maximum output of wind turbine
$P_{\mathrm{PV},j}$	active output of jth photovoltaic unit
$k_{\mathrm{PV},j}$	cost coefficient of jth photovoltaic unit
N_{PV}	number of photovoltaic units
N_{WT}	number of wind turbines
$f(P)$	beta function
α, β	shape parameters that uniquely define beta-function characteristic
$A(\alpha, \beta)$	normalization function.
η/σ^2	expectation/variance of beta function
$\phi(t)$	prediction error of current time period
N_{col}	number of WP output data points
$F_{\mathrm{fuel}}/F_{\mathrm{run}}$	gas fuel cost/equipment operation and maintenance cost for CCHP microgrid
F_{grid}	cost of CCHP microgrid to interact with external electricity grid
η_{MT}	gas turbine power generation efficiency
a, b, c, d	parameters determined by gas turbine unit
w_{LNG}	alorific value of gas
$Q_{\mathrm{GT}}(t)$	residual heat in flue gas emitted as waste heat by gas turbine
η_{ST}	gas turbine power generation efficiency
$\eta_{\mathrm{ST},l}$	heat loss coefficient of gas turbine j
V_{ST}	gas consumption
$Q_{\mathrm{MT}}(t)$	residual heat in flue gas emitted as waste heat by gas turbine
$Q_{\mathrm{AH,out/in}}(t)$	output/input of waste heat boiler in period t
η_{AF}	efficiency of waste heat boiler
$Q_{\mathrm{G,out}}(t)$	output of gas boiler in period t
$G_{\mathrm{cons}}(t)$	gas consumption
η_{G}	efficiency of gas boiler
$Q_{\mathrm{HX}}(t)$	output of heat exchanger in period t
η_{HX}	efficiency of heat exchanger
$Q_{\mathrm{AC}}(t)$	output of absorption chiller in period t
η_{AC}	efficiency of absorption chiller
$Q_{\mathrm{EC}}(t)$	output of electric chiller in period t
$P_{\mathrm{EC}}(t)$	electric power consumed by electric chiller
λ_{EC}	efficiency of electric chiller
$P_{\mathrm{trans}}(t)$	electric power transferred by microgrid to external grid or adjacent microgrid during period t
$P_{\mathrm{trans,max}}$	limit of transmission line
G_{C}	price of gas
F_{G}	gas consumption of gas boiler
$P_{\mathrm{sh}}(t)/P_{\mathrm{ov}}(t)$	differences between output power
$P_{\mathrm{load}}(t)$	load power of microgrid in period t
$B_{\mathrm{p}}(t)$ / $S_{\mathrm{p}}(t)$	purchasing/selling prices of electricity
k_{MT}, k_{G}, k_{AH}	efficiency of operation and maintenance costs of gas turbine, gas boiler, and waste heat boiler, respectively
k_{HX}, k_{AC}, k_{EC}	efficiency of operation and maintenance costs of heat exchanger, absorption chiller, and electric chiller units, respectively
k_{FC}, k_{WT}, k_{PV}	efficiency of operation and maintenance costs of battery, wind farms, and PV arrays, respectively
$P_{\mathrm{AH}}(t)$, $P_{\mathrm{HX}}(t)$, $P_{\mathrm{AC}}(t)$	output power of waste heat boiler, heat exchanger, and absorption chiller, respectively
$B/S_{\mathrm{p}}(t)$	purchasing and selling prices of electricity
$f_{\mathrm{F,P}}$	pollutant emission of CCHP microgrid
$f_{\mathrm{GT},i}/f_{\mathrm{FC},i}$	pollutant discharges per unit time of ith GT and FC unit
$e_{\mathrm{GT},i}$, $g_{\mathrm{GT},i}$, $r_{\mathrm{GT},i}$	pollutant emission coefficients of ith GT unit
$e_{\mathrm{FC},i}$, $g_{\mathrm{FC},i}$, $r_{\mathrm{FC},i}$	pollutant emission coefficients of ith FC unit
$\lambda_{\mathrm{GT},i}$	raw material consumption coefficients of ith GT unit
$\lambda_{\mathrm{FC},i}$	raw material consumption coefficients of jth FC unit
$P_{\mathrm{cool}}(t)/P_{\mathrm{heat}}(t)$	cold load power and heat load power of CCHP microgrid
$P_{\mathrm{GT,min/max},i}$	minimum/maximum outputs of ith GT unit
$P_{\mathrm{FC,min/max},i}$	minimum/maximum outputs of ith FC unit
$P_{\mathrm{GT},d/u,\mathrm{max},i}$	maximum downward/upward ramping rate of ith GT unit output
$P_{\mathrm{FC},d/u,\mathrm{max},i}$	maximum downward/upward ramping rate of ith FC unit output
$Q_{\mathrm{AH,min/max}}$	minimum/maximum heat outputs of waste heat boiler
$Q_{\mathrm{G,min/max}}$	minimum/maximum heat outputs of gas boiler

$Q_{\mathrm{HT,min/max}}$	minimum/maximum heat outputs of heat exchanger
$Q_{\mathrm{AC,min/max}}$	minimum/maximum cooling capacities of absorption chiller
$P_{\mathrm{EC,min/max}}$	minimum/maximum input electric power of electric chiller
$P'_{\mathrm{wt},i}(t)$	maximum output predicted of ith wind turbine at period t

I. INTRODUCTION

Currently, clean energy sources, such as wind power (WP) and photovoltaic (PV) power, have been promoted worldwide due to their renewability and environmental friendliness. Wind and PV power are also excellent distributed generation (DG) power sources that can be easily integrated with local small-scale power grids, such as microgrids. Here, a microgrid is generally considered a small-scale generation-transmission-distribution system that combines various local DG sources, energy storage systems, and electrical loads [1]. At present, combined cooling, heating, and power (CCHP) systems that simultaneously provide cooling, heating, and power have demonstrated considerable potential for micro-scale domestic applications [2]–[4]. However, the distributed nature of microgrids requires careful dispatch planning of each of the controllable units within the grid to ensure good economic performance. The conventional economic dispatching of a microgrid mainly relies on a reasonable management of the output of each controllable unit in the grid, and it addresses the uncertainties associated with the random nature of renewable energy sources like wind and PV power as much as possible under the premise of meeting the load demand [5], while minimizing the economic losses caused by abandoned WP and PV power and the operation and maintenance cost of controllable units [6], [7]. However, the uncertainty associated with renewable energy source outputs will inevitably affect the effectiveness and accuracy of conventional microgrid economic dispatching as the increasing penetration of renewable energy sources in microgrids [8], [9]. While the output of PV power fluctuates to a relatively small degree and can be easily extrapolated from high-precision weather forecasts, the output of WP fluctuates greatly and irregularly due to the extreme randomness of wind direction and wind speed. Addressing this issue requires reasonable forecasting of wind outputs as well as more sophisticated economic dispatching methods. Research focused on WP output forecasting has achieved some reasonable results, and the forecasting methods employed can be mainly divided into simulation methods based on scenario prediction and analytic methods based on point prediction. Simulation methods based on scenario prediction employ sampling of each random uncertainty factor, and then integrate these factors into specific simulation scenarios. Then, the comprehensive influence of the probability distribution of these random variables on the objective function value and the risk value (or opportunity cost) is described according to the occurrence probability and simulation result of each scenario. An example of this method is the development of a probability model between the fatigue load of wind turbines and WP output [10]. Since each wind farm has different factors, such as topography, latitude, fan size, and the wind turbine material, there is an over-reliance on experience using simulation methods. The analytic method employs random sampling and probability statistics to obtain a more robust and universally applicable prediction model than that obtained by simulation methods [11]. In analytic methods based on point prediction, a corresponding empirical model of prediction error is established according to the prediction scale, such as a normal distribution model (NDM) or a Poisson distribution model (PDM), and its probability density function or distribution accumulation function is determined. For example, numerical methods, such as prediction functions and sampling, have been applied for constructing WP forecasting models [12]. The randomness of WP output has also been characterized in a model combining a stacked auto encoder (SAE) and a back-propagation (BP) algorithm [13]. Moreover, intelligent algorithms and fitting models have also been applied to WP prediction [10], [14]. However, these typical uses of single-layer prediction models increases the computational burden of these models, and often fails to obtain sufficiently accurate confidence probability intervals. In this paper, a beta-function-based double-layer method of forecasting wind power output and calculating error expectation is proposed that describes the uncertainty of WP output more accurately and provides the economic cost due to inaccuracy. While the topic of microgrids has generated considerable interest in recent years, microgrid research has been typically more focused on optimal planning [15], design [16], [17], and integration control [18] rather than on economic dispatch. In some research, price penalty factors are introduced in the early stages to transform the resulting multi-objective optimization problem into a single-objective optimization problem [19], [20]. Nonetheless, these methods have failed to reflect the trade-off between economic and environmental objectives in the optimization process, and the price penalty factor value is often set based on the individual experience of the researcher, which is not an objective basis. By optimizing all of the objectives during each iteration, multi-objective EEDs can avoid inappropriate parameter selection due to insufficient experience of researchers. Currently, many methods are used to solve multi-objective EEDs, such as self-learning teaching-learning based optimization (TLBO) [21] and the technique for order preference by similarity to solution (TOPSIS) [22]. However, these methods often use only one single population to represent all of the decision variables in the actual optimization process. The coordinated relationship of each controllable unit in the microgrid is not fully considered in these solution processes [19]–[22], resulting in a high probability of obtaining a locally convergent solution with low computational efficiency. Co-evolutionary optimization algorithms have recently provided a new means of solving multi-objective optimization problems for microgrids. The term co-evolution was first

proposed by Ehrlich and Raven in 1964 when discussing the evolutionary effects of plants and herbivores [23]. In 1980, Janzen provided a strict definition of co-evolution: the reciprocal adaptation of two or more interacting species [24]. In other words, co-evolution is the evolution of the reaction of traits. Co-evolutionary algorithms are often combined with other algorithms, such as the co-evolutionary genetic algorithm that combines a co-evolutionary algorithm with a classical genetic algorithm. Co-evolutionary optimization algorithms are therefore iterative algorithms inspired by the mutual cooperation and competition among biological populations in the biological world. For example, the introduction of a co-evolutionary theory framework into electric power systems and the electricity market has been demonstrated to provide a new method of optimal planning and operation of electric power systems [25]. However, the application of co-evolutionary optimization algorithms in microgrids mainly focuses on microgrid control and the electricity market [26], [27], which means that the research on multi-objective environmental/economic dispatch of CCHP microgrids based on co-evolutionary optimization is necessary and interesting. In summary, this paper seeks to address all of the above-discussed problems simultaneously by proposing a CCHP microgrid economic dispatch model with multiple types of power output units based on the time-of-use (TOU) price in conjunction with a double-layer wind power output forecasting error expectation, which describes the uncertainty of WP output more accurately. A co-evolutionary optimization algorithm is combined with the non-dominated sorting genetic algorithm (NSGA-II) to greatly improve the global search ability and convergence performance of the NSGA-II, which is named the CoNSBAS algorithm. A practical microgrid system in Northwest China is simulated as a case study, and the performance of the proposed algorithm is compared with that of the conventional NSGA-II. The simulation results demonstrate the superiority of the global search performance and the rapid convergence of the improved optimization algorithm.

II. REAL-TIME WIND POWER OUTPUT PROBABILITY PREDICTION MODEL

A. BETA-FUNCTION MODEL OF WIND POWER OUTPUT

As discussed above, the dramatic fluctuation of WP output has a considerable impact on the economic dispatch of microgrids. However, a full consideration of the impact of WP output uncertainty on economic dispatch requires the application of the Monte Carlo simulation method to fit the WP output probability distribution [28]. Moreover, it has been proved that the characteristics of wind power output can be well expressed by the beta function [29]. To this end, this paper models the WP output probability distribution using a beta function. Because the processing range of the beta function is [0, 1] and the actual range of WP output is $[0, \infty)$, we must first normalize the WP output probability distribution data. To demonstrate the characteristics of WP output, Fig. 1 shows the WP output data of 200 points at a particular time in a day

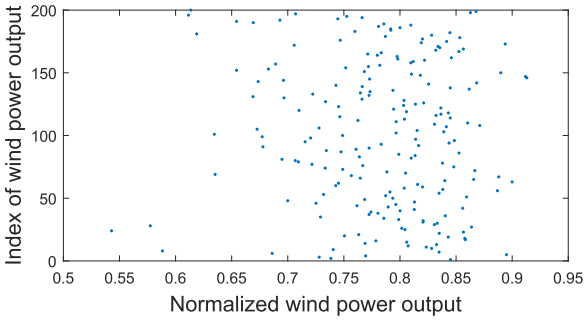

FIGURE 1. Active power output of wind turbines in actual wind farm.

for an actual wind farm. The normalization and fitting process is described as follows.

First, the wind farm output is normalized as follows.

$$h_{\mathrm{wt},i}(t) = \frac{P_{\mathrm{wt},i}(t)}{P_{\mathrm{theory-max,wt}}}. \tag{1}$$

$$u_{\mathrm{wt},i}(t) = \frac{P'_{\mathrm{w,i}}(t)}{P_{\mathrm{theory-max,wt}}}. \tag{2}$$

We divide the normalized range of [0, 1] into γ regions, $\left[0, \frac{1}{\gamma}, \ldots, \frac{\gamma-1}{\gamma}, 1\right]$, and calculate the prediction error of the current time period according to $h_{\mathrm{wt},i}(t)$ and $u_{\mathrm{wt},i}(t)$:

$$\phi(t) = h_{\mathrm{wt},i}(t) - u_{\mathrm{wt},i}(t). \tag{3}$$

The real-time WP output probability is then expressed by a beta function as follows.

$$f\left(h_{\mathrm{wt},i}\right) = \frac{{h_{\mathrm{wt},i}}^{\alpha-1}\left(1-h_{\mathrm{wt},i}\right)^{\beta-1}}{A(\alpha,\beta)}. \tag{4}$$

$$A(\alpha,\beta) = \int_0^1 h_{\mathrm{wt},i}^{\alpha-1}\left(1-h_{\mathrm{wt},i}(t)\right)^{\beta-1} dh_{\mathrm{wt},i}. \tag{5}$$

According to the nature of the beta distribution, the expectation function η, predicted variance σ^2, and parameters α and β have the following functional relationships.

$$\begin{cases} \eta = \dfrac{\alpha}{\alpha+\beta} \\ \sigma^2 = \dfrac{\alpha\beta}{(\alpha+\beta+1)(\alpha+\beta)^2} \\ \eta = \dfrac{1}{N_{\mathrm{col}}}\displaystyle\sum_{i=1}^{N_{\mathrm{col}}} P_{\mathrm{wt},i} \\ \sigma^2 = \dfrac{1}{N_{\mathrm{col}}-1}\displaystyle\sum_{i=1}^{N_{\mathrm{col}}}\left(P_{\mathrm{wt},i}-\eta\right)^2 \end{cases}. \tag{6}$$

$$\alpha = \frac{(1-\eta)\eta^2}{\sigma^2} - \eta. \tag{7}$$

$$\beta = \frac{1-\eta}{\eta}\alpha. \tag{8}$$

Here, N_{col} is the number of WP output data points. The specific derivation is shown elsewhere [5].

The limitations of existing prediction algorithms and data recording methods make it unreasonable to predict WP

output with 100% accuracy. Therefore, this paper employs a confidence level p of 95%. Next, the concept of WP over-scheduling and under-scheduling must be introduced. The compensation due to inaccurate forecasting is expressed in the form of economic costs [31].

B. COMPENSATION DUE TO INACCURATE FORECASTING

As discussed above, the microgrid dispatching system is scheduled according to the WP forecast curve. Therefore, error in the WP forecast curve due to the randomness of WP output will inevitably affect the power supply accuracy because $h_{\mathrm{wt},t}(t)$ may not be equal to $u_{\mathrm{wt},t}(t)$. The two cases in which $h_{\mathrm{wt}}(t) > u_{\mathrm{wt},t}(t)$ and $h_{\mathrm{wt},i}(t) < u_{\mathrm{wt},i}(t)$ are denoted over-scheduling and under-scheduling, respectively. When $h_{\mathrm{wt},t}(t) > u_{\mathrm{wt},t}(t)$, accepting all WP output may cause safety issues. Therefore, grid companies may issue abandonment commands for capacities exceeding the grid-connected technical standards. However, encouraging the development of WP requires that wind farms be fairly compensated for WP output abandonment by grids. However, to encourage the development of WP, it is necessary to compensate wind farms fairly for WP output abandonment by grids [32]. Contrary to the case of overscheduling, $h_{\mathrm{wt},i}(t)$ is completely acceptable when $h_{\mathrm{wt},t}(t) < u_{\mathrm{wt},t}(t)$, while under-scheduling conditions require that the automatic gain control (AGC) be adjusted or that standby units be activated to meet the load demand. Grid companies may also need to purchase high-priced electricity in the real-time power auxiliary service market.

The current approach for applying a predictive model to account for random WP outputs typically adopts a number of predictive output intervals of equivalent periods [33], and allocates equal computing resources for each interval. However, the actual WP data shown in Fig. 1 indicate that the WP output is mainly concentrated within a specific range, and some sub-intervals are observed with extremely low probability of WP output over the entire sub-interval, such as [0, 0.4] and [0.98, 1]. Moreover, the length of intervals over which the WP output is relatively dense, such as [0.4, 0.98], are very large, which results in excessively low output prediction accuracy that leads to excessive under-scheduling costs.

This paper addresses these issues by proposing the following four-step method for dynamically dividing the predicted WP output range based on historical WP output. However, we must first define the following three WP output intervals:

i) overall output interval $\boldsymbol{K} = [0, 1]$, including all possible WP output values;

ii) upper output interval $\boldsymbol{K}' = [P_{\mathrm{wt,min}\,p=95\%}, P_{\mathrm{wt,max},p=95\%}]$ $\left(\boldsymbol{K}' \subseteq \boldsymbol{\Lambda}\right)$, including the possibility of 95% WP output values

iii) lower output intervals $\boldsymbol{K}_i' = \left[P_{\mathrm{la},i} P_{\mathrm{ex},i}\right] (i = 1, \cdots, N\ \boldsymbol{K}_i'' \subseteq \boldsymbol{K}')$, are a subset of the upper output range that is used to predict WP output more accurately, where $P_{\mathrm{la},i}$ and $P_{\mathrm{ex},i}$ are the lower and upper limits of the output uncertainty set for lower output interval i.

Then, WP curve prediction and the calculation of compensation due to inaccurate forecasting are conducted as follows.

1) Set a number $N = 24$ of lower intervals. 2) The upper interval $\left[P_{\mathrm{wt\,min}\,p=95\%}, P_{\mathrm{wt.max}\,p=990^{\circ}}\right]$ is determined according to $p = 95\%$. The maximum distribution accuracy of WP output is achieved by minimizing the length of the upper interval:

$$\min dis = P_{\mathrm{wt,max},p=95\%} - P_{\mathrm{wt,min},p=95\%}. \tag{9}$$

with the following constraints.

$$0 \le P_{\mathrm{wt,min}} < P_{\mathrm{wt,max}} \le 1. \tag{10}$$

$$\sum_{i=1}^{N_{\mathrm{cal}}} \frac{\varepsilon\left(P_{\mathrm{wt},i} - P_{\mathrm{wt,min}}\right) \varepsilon\left(P_{\mathrm{wt\ max}} - P_{\mathrm{wt},i}\right)}{N_{\mathrm{col}}} \times 100\% = 95\%. \tag{11}$$

Here, N_{col} is taken as 20,000 in this paper, and $\varepsilon(\cdot)$ is a step function.

3) Minimization is conducted using the particle swarm optimization (PSO) algorithm. For the data presented in Fig. 1, the minimum normalized WP upper output interval satisfying $p = 95\%$ is [0.4871, 0.9699].

4) Establish 24 beta-function intervals for the WP upper output interval [0.4871, 0.9699] with interval lengths of 0.02, and fit the WP output data to obtain a fitting curve with sufficient credibility. Each beta-function curve represents a predicted output within the output probability distribution function. Therefore, the power supply company will give the user side total WP compensation due to inaccurate forecasting Y according to the following formula [34].

$$Y = \sum_{t=1}^{T} \sum_{i=1}^{N} \int_{\mathrm{P'_{wt}(t)}}^{P_{\mathrm{ex},i}} k_{\mathrm{ex}} \left(P - P'_{\mathrm{wt}}(t)\right) f(P) dP + \sum_{t=1}^{T} \sum_{i=1}^{N} \int_{P_{\mathrm{la},i}}^{P'_{\mathrm{wt}}(t)} k_{\mathrm{la}} \left(P'_{\mathrm{wt}}(t) - P\right) f(P) dP. \tag{12}$$

Here, $k_{\mathrm{ex},i}$ and $k_{\mathrm{la},i}$ are the over-scheduling and under-scheduling compensation coefficients of wind farm i respectively, which are related to the market environment, and T is the scheduling period, which is set to 24h in a day. Accordingly, the WP uncertainty obtained by the beta function is given as follows..

$$\phi = \sum_{j=1}^{T} \left(P_{\mathrm{ex},i} - P_{\mathrm{la},i}\right). \tag{13}$$

III. CCHP MICROGRID MULTI-OBJECTIVE UNIT OPTIMIZATION MODEL

The CCHP microgrid system optimization economic dispatch model established in this paper takes three objectives of the microgrid system as the optimization goal, and considers the constraints to optimize outputs of all of the controllable devices in the microgrid. The specific structure of a standard microgrid system is illustrated in Fig. 2.

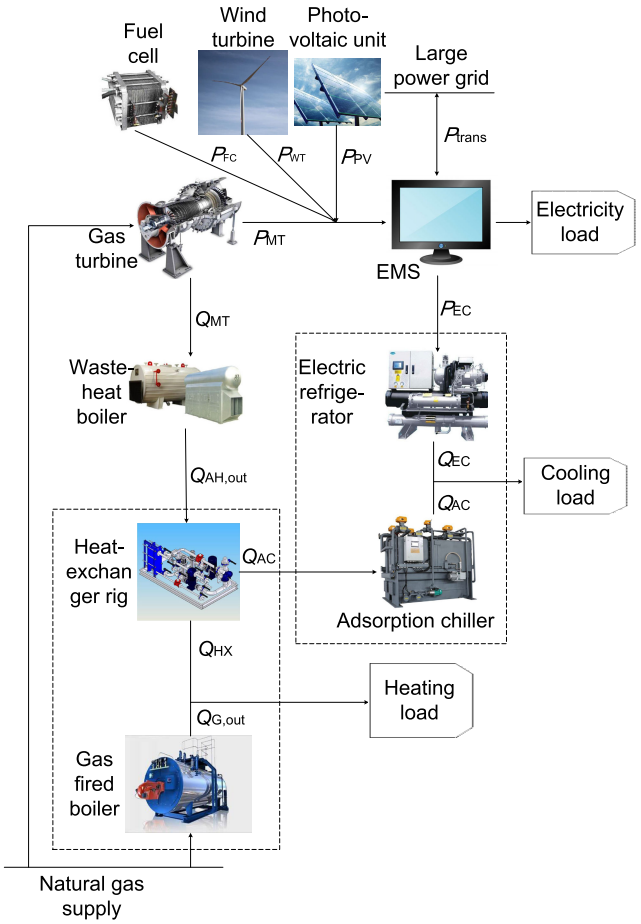

FIGURE 2. Topology of standard CCHP microgrid.

A. CCHP MICROGRID MODELING

In this paper, the CCHP microgrid is regarded as a whole. During the scheduling period, the microgrid system meets its own load requirements and specifies a schedule for each decision variable, so that the power generation cost, pollutant emission, and degree of power generation unit output asynchrony are at a minimum.

1) OPERATING COSTS

The objective function for the total operating cost F of the CCHP microgrid system is expressed as follows:

$$\min F = F_{\text{fuel}} + F_{\text{run}} + F_{\text{grid}} + Y. \tag{14}$$

These specific costs are defined for the microgrid as follows.
Gas turbine

Gas turbines are often considered to be the core equipment in CCHP systems due to their excellent electric power and heat output capabilities. The waste heat obtained while generating electric power can provide heat energy to each energy conversion unit through a corresponding collection device to meet both heat and cold loads in the network area. In the absence of external factors, the gas turbine power generation efficiency η_{GT} can be expressed by a cubic polynomial of the load rate δ :

$$\eta_{GT} = a\delta^3 - b\delta^2 + c\delta + d. \tag{15}$$

The gas consumption V_{GT} is given as:

$$V_{GT} = \frac{\sum_{t=1}^{T} P_{GT}(t)}{\eta_{GT} w_{LNG}}. \tag{16}$$

where w_{LNG} is taken as $9.7(\text{kW}\cdot\text{h})/\text{m}^3$. The residual heat $Q_{GT}(t)$ in the flue gas emitted as waste heat by the gas turbine is given as.

$$Q_{GT}(t) = P_{GT}(t)\frac{1-\eta_{GT}-\eta_{GT,l}}{\eta_{GT}}. \tag{17}$$

Waste heat boiler The waste heat of gas turbines is collected by the waste heat boiler to supply the cold and heat load requirements of the CCHP microgrid system. The output of the waste heat boiler, $Q_{AH,out}(t)$, in period t is determined by the input heat $Q_{AH,in}(t)$ and the efficiency η_{AF} of the waste heat boiler:

$$Q_{AH,out}(t) = Q_{AH,in}(t)\eta_{AF}. \tag{18}$$

Gas boiler

When $Q_{AH,in}(t)$ is insufficient to supply the heat and cold load requirements of the co-supply system, the additional heat required is supplied by burning gas in the gas boiler. The output of the gas boiler, $Q_{G,out}(t)$, in period t is determined by the gas consumption $G_{cons}(t)$ and the efficiency η_G of the gas boiler:

$$Q_{G,out}(t) = G_{cons}(t) w_{LNG}\eta_G. \tag{19}$$

Steam heat exchanger

The heat exchanger converts the steam heat of the waste heat boiler to supply the heat load demands of the system. The output of the heat exchanger, $Q_{HX}(t)$, in period t is determined by the heat output of the waste heat boiler supplied to the heat exchanger to meet the heat loads of the system and the efficiency η_{HX} of the heat exchanger:

$$Q_{HX}(t) = Q_{AH.H}(t)\eta_{HX}. \tag{20}$$

Absorption chiller

The absorption chiller employs the heat in the waste heat boiler to supply the cooling load demands of the system. The output of the absorption chiller, $Q_{AC}(t)$, in period t is determined by the heat output of the waste heat boiler supplied to the absorption chiller to meet the cold loads of the system and the efficiency η_{AC} of the absorption chiller:

$$Q_{AC}(t) = Q_{AH,C}(t)\eta_{AC}. \tag{21}$$

Electric chiller

When the output of the absorption chiller is insufficient to supply the cold loads of the system, the additional cooling is provided by the electric chiller by consuming electric power. The output of the electric chiller, $Q_{EC}(t)$, in period t is

determined by the electric power consumed by the electric chiller $P_{EC}(t)$ and its efficiency λ_{EC} :

$$Q_{EC}(t) = P_{EC}(t)\lambda_{EC}. \tag{22}$$

Wind turbine Because WP is a clean energy source, it generally has no associated environmental compensation cost, such that only the depreciation cost and operation and maintenance costs are generally considered. In the life cycle of wind farm equipment, the power generation cost C_{WT} is generally considered to have a linear relationship with the active output [35], [36]:

$$C_{WT} = \sum_{j=1}^{N_{WT}} P_{WT,j} k_{WT,j}. \tag{23}$$

Photovoltaic Array

Similar to WP, PV power is also a clean energy source, and generally has no associated environmental costs. Its comprehensive operating costs mainly include depreciation costs and operation and maintenance costs. When PV panels function normally, the PV pover generation cost C_{PV} is generally considered to have a linear relationship with the active output:

$$C_{PV} = \sum_{j=1}^{N_{PV}} P_{PV,j} k_{PV,j}. \tag{24}$$

Electric power interactions with an external electrical grid

The CCHP microgrid purchases electric power from an external grid or an adjacent microgrid when the DG power sources in the microgrid (i.e., gas turbines, wind farms, and PV arrays) cannot meet its total electric load demand. Similarly, the microgrid sells electricity to an external grid or an adjacent microgrid when the electric power generated by the microgrid is greater than its total electric load demand. The corresponding constraints that must be met are given as follows:

$$-P_{\text{trans , max}} \le P_{\text{trans}}(t) \le P_{\text{trans, max}}. \tag{25}$$

If $P_{\text{trans}}(t) > 0$, the microgrid purchases electricity, and, if $P_{\text{trans}}(t) < 0$, electricity is sold. The gas cost of the CCHP microgrid is given as:

$$F_{\text{fuel}} = \sum_{t=1}^{T} \left(\frac{G_c P_{GT}(t)}{\eta_{GT} w_{LNG}} + G_c F_G(t) \right) \tag{26}$$

The costs of interactions with external electric power grids F_{grid} are determined by the deviation Pun(t) between the output and load of the microgrid and the purchasing and selling price of electricity at each moment, which are given as follows:

$$\begin{cases} F_{\text{grid}} = \sum_{t=1}^{T} P_{\text{sh}}(t) Bp(t) - \sum_{t=1}^{T} P_{\text{ov}}(t) Sp(t) \\ P_{\text{un}}(t) = P_{\text{load}}(t) - \sum P_{GT}(t) - \sum P_{FC}(t) \\ \qquad - \sum P_{WT}(t) - \sum P_{PV}(t) \\ P_{\text{sh}}(t) = \begin{cases} P_{\text{un}}(t), & P_{\text{un}} > 0 \\ 0, & P_{\text{un}} \le 0 \end{cases} \\ P_{\text{ov}}(t) = \begin{cases} -P_{\text{un}}(t), & P_{\text{un}} \le 0 \\ 0, & P_{\text{un}} > 0 \end{cases} \end{cases} \tag{27}$$

Here, $P_{\text{sh}}(t)$ and $P_{\text{ov}}(t)$ are the differences between the output power, given as $P_{GT}(t)$, $P_{FC}(t)$, $P_{WT}(t)$, and $P_{PV}(t)$ which are those of the gas turbines, batteries, wind farms, and PV arrays, respectively, and the load power $P_{\text{load}}(t)$ of the microgrid in period t, which represent deficit and excess states of output, respectively. Equipment operation and maintenance costs of the CCHP microgrid in period t are given as follows.

$$\begin{aligned} F_{\text{run}} = & \sum_{t=1}^{T} k_{GT} P_{GT}(t) + k_G P_G(t) + k_{AH} P_{AH}(t) \\ & + k_{HX} P_{HX}(t) + k_{AC} P_{AC}(t) + k_{EC} P_{EC}(t) \\ & + k_{WT} P_{WT}(t) + k_{PV} P_{PV}(t) + k_{FC} P_{FC}(t). \end{aligned} \tag{28}$$

2) POLLUTANT EMISSIONS

The total pollutant emission of the CCHP microgrid in period t is given as.

$$f_{F,P} = \sum_{t=1}^{T} \sum_{i=1}^{N_{GT}} f_{GT,i} + \sum_{t=1}^{T} \sum_{i=1}^{N_{FC}} f_{FC,i}. \tag{29}$$

The main pollutants are carbon dioxide (CO_2), sulfur dioxide (SO_2) , and nitrogen oxides (NO,). For convenience of comparison, only the NOx emissions are considered in this paper. According to the operating data of thermal power units, the pollutant emissions of single gas turbine units and diesel units can be described by quadratic functions of their active power generation, which are given respectively as follows.

$$f_{GT,i} = e_{GT,i} P_{GT,i}^2 + g_{GT,i} P_{GT,i} + r_{GT,i}. \tag{30}$$

$$f_{FC,i} = e_{FC,i} P_{FC,i}^2 + g_{FC,i} P_{FC,i} + r_{FC,i}. \tag{31}$$

3) DEGREE OF POWER GENERATION UNIT OUTPUT ASYNCHRONY

The incremental rate gas cost increases with increasing active power output within the normal load range. Therefore, the service life of a single unit will be seriously affected if it must disproportionally bear the output of the microgrid for that type of unit. Therefore, this paper introduces the following function to represent the degree of output asynchrony for

a given type of unit.

$$f_{di} = \sum_{i=1}^{N_{cr}} \sum_{j=1;j\neq i}^{N_{cr}} \left(\lambda_{\mathrm{GT},i} P_{\mathrm{GT},i}(t) - \lambda_{\mathrm{GT},j} P_{\mathrm{GT}j}(t)\right)^2 + \sum_{i=1}^{N_{\mathrm{rec}}} \sum_{j=1;j\neq i}^{N_{\mathrm{FC}}} \left(\lambda_{\mathrm{FC},i} P_{\mathrm{FC},i}(t) - \lambda_{\mathrm{FC},j} P_{\mathrm{FC},j}(t)\right)^2. \quad (32)$$

Because a high-power unit consumes less raw material than a low-power unit for the same active power output, the raw material consumption coefficient of a high-power unit is relatively small [37].

B. CONSTRAINTS OF MULTI-OBJECTIVE OPTIMIZATION

The operating constraints of the CCHP microgrids system include constraints associated with cooling, heating, and energy balance, the constraints of equipment output, and interaction constraints with external grids, which are given as follows. Cold balance constraint:

$$P_{\mathrm{EC}}(t)\lambda_{\mathrm{EC}} + Q_{\mathrm{AC}}(t) = P_{\mathrm{cool}}(t). \quad (33)$$

Thermal balance constraint:

$$Q_{\mathrm{GB}}(t) + Q_{\mathrm{HX}}(t) = P_{\mathrm{heat}}(t). \quad (34)$$

Electrical balance constraint:

$$P_{\mathrm{load}}(t) = P_{\mathrm{GT}}(t) + P_{\mathrm{WT}}(t) + P_{\mathrm{PV}}(t) + P_{\mathrm{trans}}(t) + P_{\mathrm{FC}}(t). \quad (35)$$

The equipment operation constraints are given as follows.

$$\begin{cases} P_{\mathrm{GT,min},i} \le P_{\mathrm{GT},i}(t) \le P_{\mathrm{GT,max},i} \\ P_{\mathrm{FC,min},i} \le P_{\mathrm{FC},i}(t) \le P_{\mathrm{FC,max},i} \\ P_{\mathrm{GT},d,\mathrm{max},i} \le P_{\mathrm{GT},i}(t+1) - P_{\mathrm{GT},i}(t) \le P_{\mathrm{GT},u\,\mathrm{max},i} \\ P_{\mathrm{FC},d,\mathrm{max},i} \le P_{\mathrm{FC},i}(t+1) - P_{\mathrm{FC},i}(t) \le P_{\mathrm{FC,umax},i}. \end{cases} \quad (36)$$

$$Q_{\mathrm{AH,min}}(t) \le Q_{\mathrm{AH}}(t) \le Q_{\mathrm{AH,max}}(t). \quad (37)$$

$$Q_{\mathrm{G,min}} \le Q_{\mathrm{G,out}}(t) \le Q_{\mathrm{G,max}}. \quad (38)$$

$$\begin{cases} Q_{\mathrm{HX,min}} \le Q_{\mathrm{HX}}(t) \le Q_{\mathrm{HX,max}} \\ Q_{\mathrm{AC,min}} \le Q_{\mathrm{AC}}(t) \le Q_{\mathrm{AC,max}} \\ P_{\mathrm{EC,min}} \le P_{\mathrm{EC}}(t) \le P_{\mathrm{EC,max}}. \end{cases} \quad (39)$$

$$\begin{cases} 0 \le P_{\mathrm{wt},i}(t) \le P'_{\mathrm{wt},i}(t) \\ 0 \le P_{\mathrm{pv},i}(t) \le P'_{\mathrm{pv},i}(t). \end{cases} \quad (40)$$

IV. HYBRID MULTI-OBJECTIVE OPTIMIZATION ALGORITHM

A. COOPERATIVE CO-EVOLUTION THEORY

According to the principle of co-evolution, the final solution obtained in a game is a Nash equilibrium, where, in a game $G = \{S_1, \cdots, S_n : u_1, \cdots, u_n\}$, for any strategy group$(S_1^*, \cdots, S_n^*)$ consisting of each strategy of each player, the strategy S_i^* of game party i is the best countermeasure against the combination of the other game party strategies $\left(S_1^*, \cdots, S_{i-1}^*, S_{i+1}^*, \cdots, S_n^*\right)$. This is denoted as follows.

$$u_i\left(S_1^*, \cdots, S_{i-1}^*, S_i^*, S_{i+1}^*, \cdots S_n^*\right) \le u_i\left(S_1^*, \cdots, S_{i-1}^*, S_{ij}^*, S_{i+1}^*, \cdots S_n^*\right). \quad (41)$$

Therefore, $\left(S_1^*, \cdots, S_n^*\right)$ is a Nash equilibrium of G for any $S_{ij} \in S_i$. The various populations learn from each other in the process of obtaining the Nash equilibrium, and continuously reconstruct their performance to make them finally tend toward a globally optimal solution.

B. NON-DOMINATED SORTING GENETIC ALGORITHM

1) PARETO OPTIMALITY SOLUTION

Multi-objective optimization problems have multiple optimization targets, where each is represented by an objective function, and are therefore quite different from single-objective optimization problems. Here, a solution that optimizes all objective functions simultaneously is quite difficult to obtain because there is no conflict between the multiple targets. Therefore, the optimization of multi-objective problems typically adopt a solution set, which contains solutions that are incomparable among the various objective functions, and which is characterized by an inability to improve the result of any objective function without weakening the results of at least one other objective function. Such solutions are denoted non-dominated solutions or Pareto optimality solutions. This condition generally holds in power systems that function within a complex operating environment, and usually require the optimized scheduling of complex objective functions. For example, the multi-objective EED optimizations required in a CCHP microgrid system cannot be solved analytically due to their unique mathematical forms.

2) NSGA-II

The basic operation of the NSGA-II is given according to the following five steps.

(1) Initialize the individuals in the population V by randomly assigning values for all of the decision variables in each individual $\mathbf{x} = [x_1 x_2 \ldots x_n]^{\mathrm{T}}$. Then, calculate the target benefits of each initial individual according to the objective functions, and perform non-dominated sorting on the premise of satisfying the applicable constraints.

(2) Assuming m objective functions, the individuals $\mathbf{x}_j$ are sequentially sorted according to their i th objective function values $f_{i,j}$. For all other individuals $\mathbf{x}_k, k \neq j$, if $f_{f,j} \le f_{i,k}$ (the target is to minimize the objective function) or $f_{i,j} \ge f_{i,k}$ (the target is to maximize the objective function) are always true, then the degree of dominance of individual $\mathbf{x}_j$ is 0, which is the current optimal solution. If $f_{i,j} = f_{k,j}$ is always true for the $(m-1)$ th objective function of one individual $\mathbf{x}_k, k \neq j$, and $f_{m,j} \ge f_{m,k}$ (the goal of this paper is to minimize the objective function), the non-dominance of individual $\mathbf{x}_j$ is 1.

(3) Lower-cost, low-asynchrony, and low-pollution individuals are given higher dominance, and form several non-dominated layers.

(4) According to the m objective functions, the population of individuals in each non-dominated layer are sequentially ordered according to the following formula:

$$L(x_i) = \sum_{d=1}^{m} \frac{f(x_{i+1})_d - f(x_{i-1})_d}{f_d^{\max} - f_d^{\min}}. \quad (42)$$

(5) Generate new population $\boldsymbol{V}$' according to cross-probability η_{cr} and mutation probability η_{mu}, which are generally 0.5 and 0.02, respectively.

(6) Calculate the corresponding objective function values and crowding distances for each individual of offspring population $\boldsymbol{V}$' Generate a temporary population by combining $\boldsymbol{V}$', and $\boldsymbol{V}$, and conduct non-dominated sorting of the temporary population.

(7) Select the highest-performing individuals from the temporary population as the new $\boldsymbol{V}$ according a set ratio, which is 0.5.

(8) If the optimization condition is met, terminate iterations and record the optimal variable values; otherwise, return to step (2).

3) DEFECTS IN CURRENT NSGA-II

In the current NSGA-II, populations with different degrees of dominance cannot be further compared. This may lead to the exclusion of individuals with poor fitness, but with a high potential to yield subsequent generations of individuals with excellent fitness. Therefore, the global search capability of the NSGA-II has room for improvement.

C. DEFECTS IN CURRENT NSGA-II

The beetle antennae search (BAS) algorithm is an intelligent optimization algorithm proposed by Jiang and Li in 2017 that was inspired by the foraging process of longhorn beetles. Here, a beetle searching for food has no certain knowledge regarding the locations of food sources. However, the general location can be determined based upon the information received by its two long antennae. If the intensity of the scent received by the left antenna is greater than that received by the right antenna, the beetle will fly to the left; otherwise, it will fly to the right. The beetle can eventually locate food by applying this principle iteratively. The BAS algorithm flow for the z-dimensional CCHP microgrid system optimization problem is described by the following five steps.

(1) Eight optimization variables are selected in this paper: the output power $P_{\mathrm{GT}}(t)$ of each of the four small gas turbines, the output power $P_{\mathrm{FC}}(t)$ of the two fuel cell units, the grid tie line power $P_{\mathrm{trans}}(t)$, and the heat distribution rate w. We assign z-dimensional vectors $\mathbf{x}_l$ and $\mathbf{x}_r$ to the left antenna and right antenna, respectively, and the distance between the two antennae is d.

(2) The orientation of the beetle is random, so a random z -dimensional unit vector is generated to represent $\mathbf{x}_l$ and $\mathbf{x}_r$.

$$\vec{r} = \frac{rands(z,1)}{\|rands(z,1)\|}. \tag{43}$$

where $rands(z, 1)$ represents a random vector generated in z dimensions. Therefore, we respectively define $\mathbf{x}_l$ and $\mathbf{x}_r$ in successive iterations as follows:

$$x_{\lambda+1,l} = x_\lambda + d_\lambda \vec{r}. \tag{44}$$

$$x_{\lambda+1,r} = x_\lambda - d_\lambda \vec{r}. \tag{45}$$

Here, d_λ is the distance between the two antennae and $\mathbf{x}_\lambda$ is the position of the centroid of the beetle at the λ th iteration.

(3) Calculate the respective fitness values f_l and f_r of $\mathbf{x}_l$ and $\mathbf{x}_r$, and determine the subsequent direction of the beetle according to the relationship between f_l and f_r :

$$x_\lambda = x_{\lambda-1} - \delta_{\lambda-1} \cdot b \cdot \mathrm{sign}\left(f_l^{\lambda-1} - f_r^{\lambda-1}\right). \tag{46}$$

where *sign* is the sign function and δ_λ is the step size of beetle motion at the λ th iteration.

(4) Calculate the fitness value after completing the beetle motion, and update d and δ as follows:

$$d_\lambda = eta_d d_{\lambda-1}. \tag{47}$$

$$\delta_\lambda = eta_\delta \delta_{\lambda-1}. \tag{48}$$

Here, eta_d and eta_δ are the attenuation coefficients for d and δ, respectively, which are both usually 0.95.

(5) If the optimization condition is met, terminate iterations and record the optimal variable values; otherwise, return to step (2).

D. CoNSBAS ALGORITHM

The co-evolutionary framework and the BAS algorithm are combined to establish complex populations based on steps (1)-(5) of the NSGA-II, and mutual cooperation and learning are conducted. In the solution method of CCHP microgrids in this paper, the output of N_{GT} gas turbines, output of N_{FC} fuel cell units, power of transmission line, and heat distribution ratio in the waste heat boiler are selected as decision variables. Thus, two q-dimensional cooperative populations $\boldsymbol{A}$ and $\boldsymbol{B}$ are established, where $\boldsymbol{A}$ represents the outputs of N_{GT} gas turbines and $\boldsymbol{B}$ the outputs of N_{FC} fuel cell units, output of N_{FC} fuel cell units, power of transmission line, and heat distribution ratio w of the waste heat boiler, which are given as follows:

$$A = \begin{bmatrix} P_{1,1} & P_{1,2} & \cdots & P_{1,N_{\mathrm{GT}}} & f_{1,1} & \cdots \\ P_{2,1} & P_{2,2} & \cdots & P_{2,N_{\mathrm{GT}}} & f_{2,1} & \cdots \\ \vdots & \vdots & & \vdots & \vdots & \\ P_{q,1} & P_{q,2} & \cdots & P_{q,N_{\mathrm{GT}}} & f_{q,1} & \cdots \end{bmatrix}$$
$$\begin{bmatrix} f_{1,m} & r_1 & L_1 \\ f_{2,m} & r_2 & L_2 \\ \vdots & \vdots & \vdots \\ f_{q,m} & r_q & L_q \end{bmatrix}$$

$$\boldsymbol{B} = \begin{bmatrix} P'_{1,1} & \cdots & P'_{1,N_{\mathrm{FC}}} & P_{1,\,\mathrm{trans}} & w_1 \\ P'_{2,1} & \cdots & P'_{2,N_{\mathrm{rc}}} & P_{2,\,\mathrm{trans}} & w_2 \\ \vdots & & \vdots & \vdots & \vdots \\ P'_{q,1} & \cdots & P'_{q,N_{\mathrm{FC}}} & P_{3,\,\mathrm{trans}} & w_q \end{bmatrix}$$
$$\begin{bmatrix} f'_{1,1} & \cdots & f'_{1,m} & r'_1 & L'_1 \\ f'_{2,1} & \cdots & f'_{2,m} & r'_2 & L'_2 \\ \vdots & & \vdots & \vdots & \vdots \\ f'_{q,1} & \cdots & f'_{q,m} & r'_q & L'_q \end{bmatrix}$$

Here, P_{ij} and P'_{ij} are the outputs of the jth group gas turbines and fuel cell unit j in the i th individual ($i = 1, \cdots, q$, $j = 1, \cdots, N'_{\mathrm{GT},j}, \cdots, N_{\mathrm{FC}}$), f_{ij} and $f_{i,j}$ are the respective fitness values of the j th objective function obtained by the ith individual of populations $\boldsymbol{A}$ and $\boldsymbol{A}$, r_i, and r_i are the respective non-dominance of the i th individual of populations $\boldsymbol{A}$ and $\boldsymbol{B}$, and L_i and L_i are the respective crowding distances of the i th individual of populations $\boldsymbol{A}$ and $\boldsymbol{B}$. Therefore, the microgrid optimization process based on the CoNSBAS algorithm is given as follows. (1) Before conducting the BAS process at each iteration, we calculate the fitness as the reciprocal of the objective function value for the first individual of population $\boldsymbol{A}$ as follows.

$$\begin{cases} f(\mathbf{x}_1)_1 = \sum_{v=1}^{q} f([\mathbf{x}_1; \mathbf{x}_v])_1 \\ f(\mathbf{x}_1)_2 = \sum_{v=1}^{q} f([\mathbf{x}_1; \mathbf{x}_v])_2 \\ \vdots \\ f(\mathbf{x}_1)_m = \sum_{v=1}^{q} f([\mathbf{x}_1; \mathbf{x}_v])_m \end{cases} \tag{49}$$

Here, individual $\mathbf{x}_1$ is combined with the q individuals of the entire population $\boldsymbol{B}$ sequentially, and the corresponding objective function $\boldsymbol{B}$ sequentially, and the corresponding objective function values are calculated according to (14), (29), and (32), respectively. These three fitness values for $\mathbf{x}_1$ are used to calculate the crowding distance of $\mathbf{x}_1$ according to (42) . Accordingly, this process is extended to the remaining individuals of populations $\boldsymbol{A}$ and $\boldsymbol{B}$. Then, the crowding distances of populations $\boldsymbol{A}$ and $\boldsymbol{B}$ are respectively calculated and subjected to non-dominated sorting according to steps (2)-(4) of the NSGA-II. (2) Then, arrange the dynamic step size of beetle motion δ_{d} and mutation probability η_{mud} for each individual $\mathbf{x}_v (v = 1, \cdots, q)$ according to the following adaptive variation formula.

$$\begin{cases} \delta(\mathbf{x}_v)_d^{\lambda} = \alpha_\delta \cdot e^{\left(1-\frac{\lambda}{\mathrm{Max}\lambda}\right)} \\ \qquad \cdot \dfrac{L(\mathbf{x}_v)^{\lambda} - L(\mathbf{x}_v)_{\min}^{\mathrm{History}}}{L(\mathbf{x}_v)_{\mathrm{Max}}^{\mathrm{History}} - L(\mathbf{x}_v)_{\min}^{\mathrm{History}}} + \beta_\delta \\ \eta_{\mathrm{mud}}\ (\mathbf{x}_v)_d^{\lambda} = \alpha_\eta \cdot e^{\left(1-\frac{\lambda}{\mathrm{Max}\lambda}\right)} \\ \qquad \cdot \dfrac{L(\mathbf{x}_v)^{\lambda} - L(\mathbf{x}_v)_{\min}^{\mathrm{History}}}{L(\mathbf{x}_v)_{\max}^{\mathrm{History}} - L(\mathbf{x}_v)_{\min}^{\mathrm{History}}} + \beta_\eta \end{cases} \tag{50}$$

Here, $L(\mathbf{x}_v)_{\max}^{\mathrm{History}}$ and $L(\mathbf{x}_v)_{\min}^{\mathrm{History}}$ are the respective maximum and minimum crovuding distances of each individual $\mathbf{x}_v$ during the iteration process, α_δ and β_δ are the variation coefficients of $\delta_{\mathbf{d}}$, and α_η and β_η are the variation coefficients of η_{mud}. Relatively high mutation and crossover opportunities are available when the population approaches a stable condition, which reduces the probability of reaching local optimal solutions.

(3) Generate offspring populations $\boldsymbol{A'}$ and $\boldsymbol{B'}$ from populations $\boldsymbol{A}$ and $\boldsymbol{B}$ according to δ_{d}, η_{cr}, η_{mud}, and the BAS algorithm.

(4) Calculate the corresponding objective function values $f_{i,m}$ and $f_{i,m}$ and crovuding distances L_i and L_i for each individual of offspring populations $\boldsymbol{A'}$ and $\boldsymbol{B'}$. Generate two temporary populations $\boldsymbol{A''}$, and $\boldsymbol{B''}$ by combining $\boldsymbol{A}$ and $\boldsymbol{A'}$, and $\boldsymbol{B}$ and $\boldsymbol{B'}$, and apply the non-dominated sorting of $\boldsymbol{A''}$ and $\boldsymbol{B''}$.

(5) Select the highest fitness individuals from $\boldsymbol{A''}$ and $\boldsymbol{B''}$ according the set ratio, and assign them as the new $\boldsymbol{A}$ and $\boldsymbol{B}$.

(6) If the optimization condition is met, terminate iterations and record the optimal variable values; otherwise, return to step (2).

(7) Cross-combine populations $\boldsymbol{A}$ and $\boldsymbol{B}$, select the individual groups with the best degree of non-domination, record the values of the objective functions corresponding to each solution, and plot the Pareto front.

A flowchart of the proposed CoNSBAS algorithm is shown in Fig. 3. The CoNSBAS algorithm has a greater complexity than the conventional NSGA-II. Therefore, a parallel computing environment is adopted in the present work to ensure that an adequate computation speed is obtained. In addition, this paper introduces a step penalty function mechanism in the calculation of the objective function to ensure that the optimization process does not exceed the limit of units, which helps maintain real-time power balance.

V. CASE ANALYSIS

A. TEST MICROGRID DESCRIPTION

This paper employs an actual grid-connected microgrid in northwestern China as an example. The micro-grid consists of four gas turbines, two fuel cell units, four wind turbines, and two PV arrays. The operating parameters of the power units are listed in Table. 1.

TABLE 1. Parameters of test microgrid power units.

Unit	Maximum output (kW)	Minimum output (kW)	Upward ramp rate (kW/h)	Downward ramp rate (kW/h)	Number of units
Gas turbine	45	0.7	22	21	4
Fuel cell	35	1	15	14	2
Wind turbine 1	10	0	8	8	2
Wind turbine 2	5	0	4	4	2
PV array	15	0	8	8	2
Transmission line	55	−50	35	35	1

The dispatching performance of the proposed CoNSBAS algorithm is verified by comparison with that obtained with the conventional NSGA-II. The scheduling period is 24 h. Considering the local micro-grid WP and PV power output characteristics, the scheduling time is selected from 00:00 to 24:00 on the same day. In the example, the iteration limits of

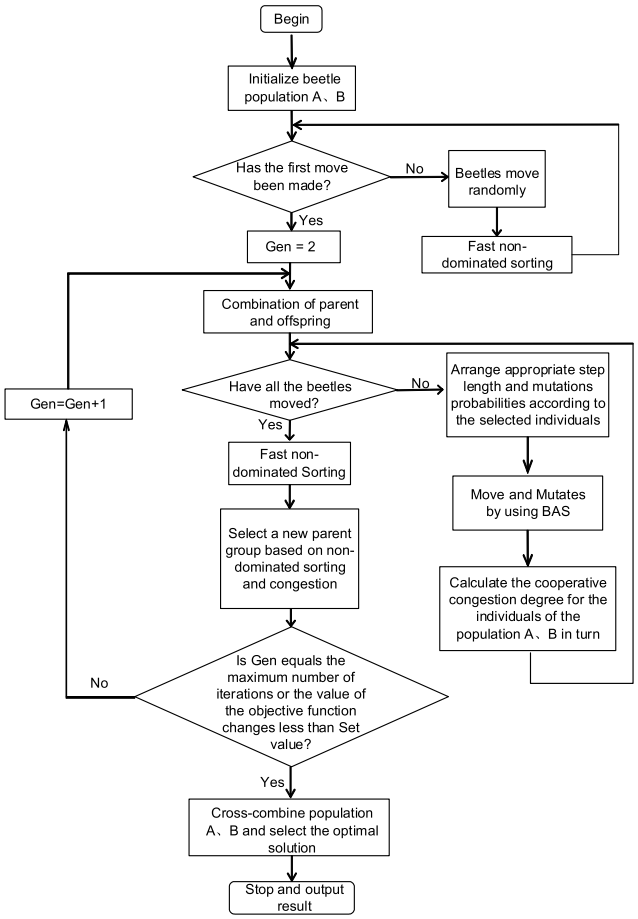

FIGURE 3. Flowchart of proposed CoNSBAS multi-objective optimization algorithm.

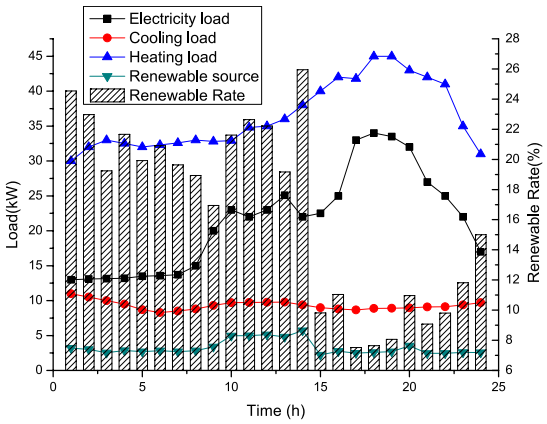

FIGURE 4. Typical daily load curves, renewable resource outputs, and renewable resource penetration rates for test microgrid.

the NSGA-II and the CoNSBAS algorithm are 40, the population sizes are 600, and the maximum power of the transmission line connecting the microgrid to the external grid is 40 kW. The predicted active load, heating load, cooling load, PV unit output, wind turbine output, and renewable energy penetration rate are shown in Fig. 4, and the time-sharing electricity transaction prices prevalent in a particular

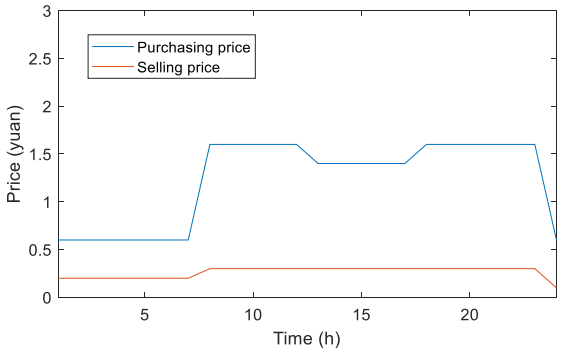

FIGURE 5. Electricity transaction prices prevalent in China during 2017.

region of China in 2017 shown in Fig. 5 were also adopted. The simulations were conducted on a personal computer with a four-core 2.6-GHz CPU and 4 GB of memory running Windows 10. The WP uncertainty model and the overall multi-objective optimization model were established using MatLab.

The thermal power unit is adopted as the main dispatching unit owing to its rapid response rate and good power regulation performance. The role of the external grid tie line is mainly to maintain the balance of power. Sudden changes in load that exceed the reaction time of the thermal power unit can be accommodated by selling excess WP and PV power to the external grid or by buying electricity from the external grid to meet deficiencies. Moreover, purchasing electricity from the external grid when the load is high can effectively address peak-to-valley differences in the load, and the peak-shaving effect is obvious.

TABLE 2. Parameters of beta probability density functions.

η	α	β	η	α	β
0.4971	22.8992	24.0381	0.7571	52.5569	16.5202
0.5971	56.4195	38.0698	0.8571	49.1216	8.1898
0.6971	38.4288	13.1735	0.9171	52.2060	4.7191

B. WIND POWER UNCERTAINTY AND COMPENSATION DUE TO INACCURATE FORECASTING

The beta-function interval was obtained according to the fitting of each WP output interval, as discussed in Section II.B, and three of the 24 WP output prediction curves are shown in Fig. 6. The parameters of these three WP output prediction curves are listed in Table. 2. Here, a normalized 95% confidence range of [0.4871, 0.9671] was employed rather than [0.4871, 0.9699] for convenience. Each lower output range is set according to the nature of the beta function, and the total WP compensation due to inaccurate forecasting given by (12) over the 24-h period was $Y = 67.98$ yuan.

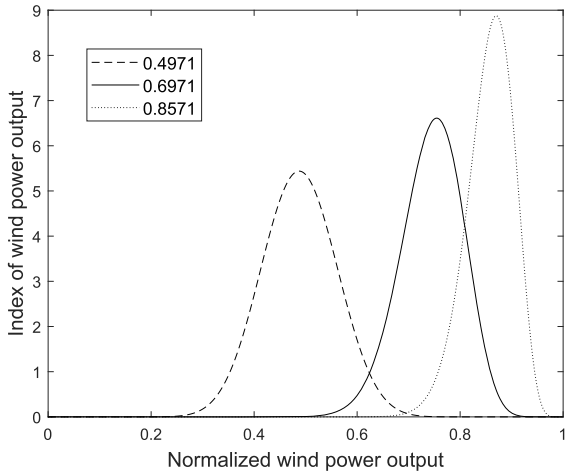

FIGURE 6. Beta probability density function examples for WP outputs.

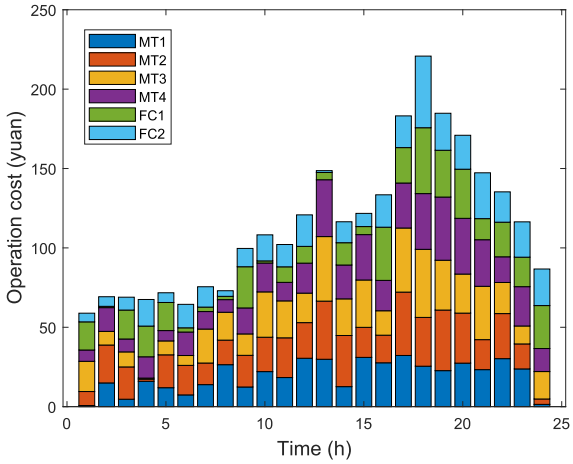

FIGURE 7. Thermal power solution provided by conventional NSGA-II algorithm.

C. COMPARISON OF MULTI-OBJECTIVE ECONOMIC DISPATCHING ALGORITHMS-PERFORMANCE

The uncertainty forecast cost of WP obtained above was adopted for conducting scheduling optimization of the test microgrid using the NSGA-II and proposed CoNSBAS algorithm. We first consider the economic cost of the microgrid over the 24-h period as the objective function to highlight the economics of the improved algorithm. The operation costs of the gas turbines and fuel cells in the test microgrid obtained by the NSGA-II are shown in Fig. 7 and those obtained by the CoNSBAS algorithm are shown in Fig. 8.

It can be seen from Fig. 4 and Fig. 7 that more WP output can be sold to the external grid for profit in the interval 00:00-07:00 due to the relatively low load of the microgrid. However, during the periods of gradually increasing load between 07:00-13:00 and 17:00-21:00, the operating costs of the thermal power units increase with increasing output, and the microgrid dispatch center will purchase electricity from the external grid if the existing units fail to

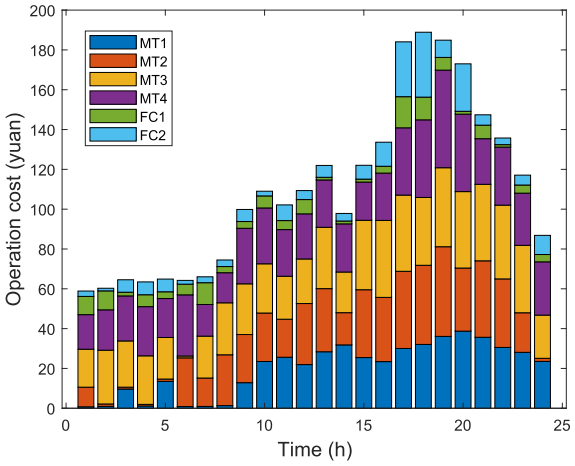

FIGURE 8. Thermal power solution provided by proposed CoNSBAS algorithm.

meet the load requirements, or if the cost of meeting those requirements is too high. It is also noted that a sharply decreasing load or increasing renewable energy output that exceeds the adjustment capability of thermal power units due to the downward ramp rate constraints would cause the microgrid dispatch center to sell electricity to the external grid.

Comparing Fig. 7 and Fig. 8, we note that the total operating cost obtained by the NSGA-II over the 24-h period was 2672.25 yuan according to (14). In contrast, the CoNSBAS algorithm obtained an operating cost of 2598.90 yuan, which reduced the overall operating cost by 2.74%. Moreover, based on the data obtained from the figures, we note that the variance of each ST and FC unit output during the 24-h period obtained by the NSGA-II was 585.49 kW^2, while the variance obtained by the CoNSBAS algorithm was 489.78 kW^2, which represents a reduction of 16.24%. This indicates that the overall outputs of the ST and FC units obtained by the CoNSBAS algorithm exhibit a reduced range of fluctuations compared with those obtained by the NSGA-II. This is conducive to the maintenance and operation of the generator set. A comparison of the active power of the transmission line obtained by the NSGA-II and the CoNSBAS algorithm is shown in Fig. 9. It can be clearly seen that the active power transmission obtained by the proposed algorithm is much more stable than that obtained by the NSGA-II, and the peak-to-valley difference is substantially reduced from 32.04 to 2.06 kW.

D. COMPARISON OF MULTI-OBJECTIVE ECONOMIC DISPATCHING ALGORITHMS-PARETO FRONT

Next, we established a multi-objective optimization model that seeks to minimize the pollutant emissions of thermal power units, degree of unit output asynchrony, and total running costs over a given period $t = 1$. In addition, the global optimization ability and convergence performance of the algorithms are compared. To this end, the final Pareto fronts

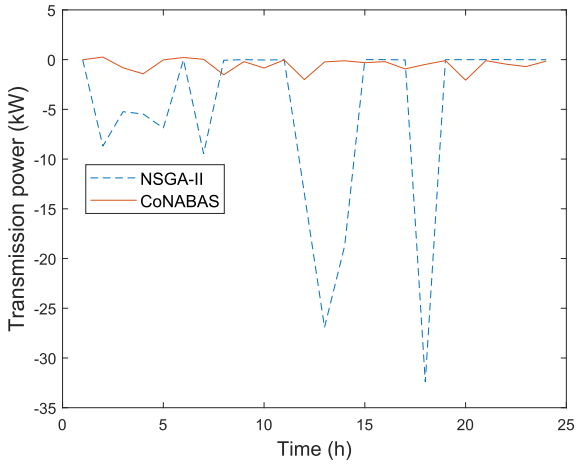

FIGURE 9. Active power of transmission line.

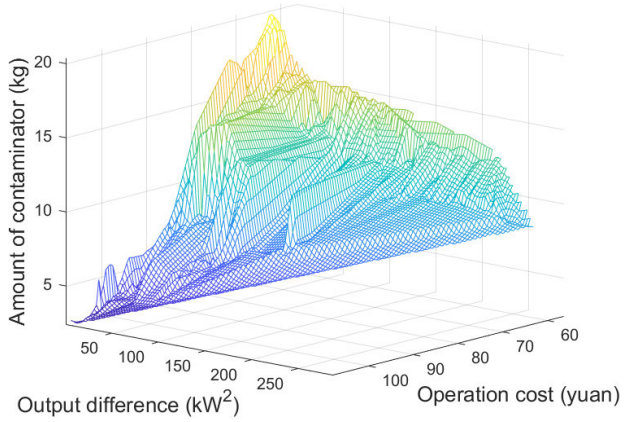

FIGURE 10. Pareto front provided by NSGA-II algorithm.

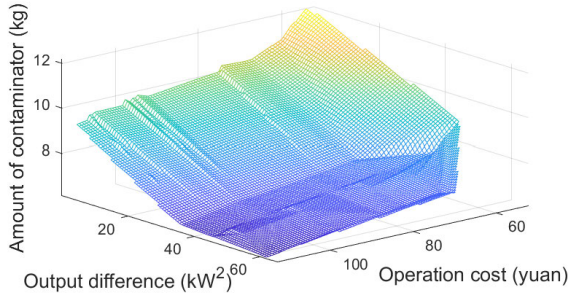

FIGURE 11. Pareto front provided by CoNSBAS algorithm.

obtained using NSGA-II and the CoNSBAS algorithm are given in Fig. 10 and Fig. 11, respectively.

It can be seen from Fig. 10 that the microgrid must depend on its own active power generation output to avoid purchasing expensive electricity from the external grid, which will lead to a substantial increase in pollutant emissions because pollutant discharge is a quadratic function of the active output.

A comparison of Fig. 10 and Fig. 11 indicates that the NSGA-II readily falls into local optimal solutions under the complex grid conditions considering WP uncertainty, and that the CoNSBAS algorithm can not only obtain the optimal solutions of the NSGA-II, but can also obtain a superior Pareto front. According to the NSGA-II calculation data, the operating cost is 81.96 yuan when the pollution emission is 8.521 kg and degree of power generation unit output asynchrony is 32.02 kW^2. Meanwhile, the operating cost obtained by the CoNSBAS algorithm is 81.96 yuan when the pollution emission is 8.53 kg and the output difference is 31.66 kW^2, which reduces the operating cost by 21.40% relative to that of the NSGA-II. Moreover, it is found that the Pareto front provided by the NSGA-II presents various irregularities, such as sudden changes, while the CoNSBAS algorithm achieves a much smoother Pareto front. At the same time, the CoNSBAS algorithm is able to obtain a stable solution with a fewer number of iterations, which is more rigorously verified in the following subsection. In addition, in the case of equivalent pollutant emissions, a decreased degree of output asynchrony means that the output of each thermal power unit corresponds to a greater extent with the raw material consumption coefficients, which reduces the consumption of raw materials and the operating cost. The Pareto front of the CoNSBAS algorithm reflects this feature much better than the NSGA-II.

E. COMPARISON OF MULTI-OBJECTIVE ECONOMIC DISPATCHING ALGORITHMS-CONVERGENCE PERFORMANCE

The convergence performance of the NSGA-II and the CoNSBAS algorithm obtained at given periods $t = 24$ h are compared in Fig. 12.

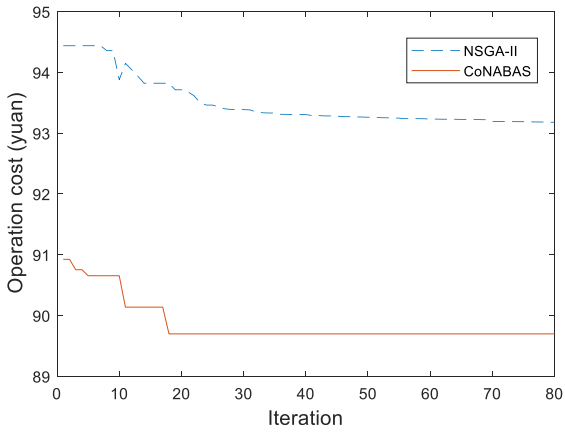

FIGURE 12. Comparison of convergence properties and computational efficiency of NSGA-II and CoNSBAS algorithm.

It can be seen from Fig. 12 that both algorithms obtain stable solutions after 65 iterations. For example, the NSGA-II obtains a stable solution after 18 iterations, while the CoNSBAS algorithm obtained a stable solution after the sixth iteration, and provides a better solution than that obtained by the NSGA-II. Therefore, the CoNSBAS algorithm is superior to the NSGA-II in terms of its convergence properties,

particularly with respect to the convergence speed and convergence result.

VI. CONCLUSION

In this paper, the dynamic partition method and the PSO algorithm were employed to delineate the upper and lower intervals of WP output. The expected WP output prediction cost was obtained by fitting the normalized WP output data to beta functions. Then, a CCHP microgrid system model based on the TOU tariff mechanism considering WP uncertainty was established. The proposed CoNSBAS algorithm combined the NSGA-II with co-evolution theory and the BAS algorithm to address the premature convergence and slow convergence of conventional NSGA-II. Finally, the effectiveness and superiority of the global optimal solution search ability and convergence performance of the CoNSBAS algorithm were verified by simulations of the modeled microgrid system in comparison with the characteristics obtained using the conventional NSGA-II.

REFERENCES

[1] P. Arboleya, C. Gonzalez-Moran, M. Coto, M. C. Falvo, L. Martirano, D. Sbordone, I. Bertini, and B. Di Pietra, "Efficient energy management in smart micro-grids: ZERO grid impact buildings," *IEEE Trans. Smart Grid*, vol. 6, no. 2, pp. 1055–1063, Mar. 2015.

[2] M. Liu, Y. Shi, and F. Fang, "Combined cooling, heating and power systems: A survey," *Renew. Sustain. Energy Rev.*, vol. 35, pp. 1–22, Jul. 2014.

[3] W. Gu, Z. Wu, R. Bo, W. Liu, G. Zhou, W. Chen, and Z. Wu, "Modeling, planning and optimal energy management of combined cooling, heating and power microgrid: A review," *Int. J. Elect. Power Energy Syst.*, vol. 54, pp. 26–37, Jan. 2014.

[4] W. Gu, Z. Wang, Z. Wu, Z. Luo, Y. Tang, and J. Wang, "An online optimal dispatch schedule for CCHP microgrids based on model predictive control," *IEEE Trans. Smart Grid*, vol. 8, no. 5, pp. 2332–2342, Sep. 2017.

[5] B. Liu, F. Zhuo, Y. Zhu, and H. Yi, "System operation and energy management of a renewable energy-based DC micro-grid for high penetration depth application," *IEEE Trans. Smart Grid*, vol. 6, no. 3, pp. 1147–1155, May 2015.

[6] M. Wu, L. J. Sun, H. Zhang, W. Wang, and G. M. Luo, "Research on optimal storage capacity of DC micro-grid system in PV station," *J. Eng.*, vol. 2017, no. 13, pp. 859–864, 2017.

[7] K. Wang, X. Huang, B. Fan, Q. Yang, G. Li, and M. L. Crow, "Decentralized power sharing control for parallel-connected inverters in islanded single-phase micro-grids," *IEEE Trans. Smart Grid*, vol. 9, no. 6, pp. 6721–6730, Nov. 2018.

[8] J. Yan, H. Zhang, Y. Liu, S. Han, L. Li, and Z. Lu, "Forecasting the high penetration of wind power on multiple scales using multi-to-multi mapping," *IEEE Trans. Power Syst.*, vol. 33, no. 3, pp. 3276–3284, May 2018.

[9] T. Surinkaew and I. Ngamroo, "Coordinated robust control of DFIG wind turbine and PSS for stabilization of power oscillations considering system uncertainties," *IEEE Trans. Sustain. Energy*, vol. 5, no. 3, pp. 823–833, Jul. 2014.

[10] Q. Yao, J. Liu, and Y. Hu, "Optimized active power dispatching strategy considering fatigue load of wind turbines during de-loading operation," *IEEE Access*, vol. 7, pp. 17439–17449, 2019.

[11] S. Fang and H.-D. Chiang, "A high-accuracy wind power forecasting model," *IEEE Trans. Power Syst.*, vol. 32, no. 2, pp. 1589–1590, Mar. 2017.

[12] Y.-K. Wu, P.-E. Su, and J.-S. Hong, "Stratification-based wind power forecasting in a high-penetration wind power system using a hybrid model," *IEEE Trans. Ind. Appl.*, vol. 52, no. 3, pp. 2016–2030, May/Jun. 2014.

[13] R. Jiao, X. Huang, X. Ma, L. Han, and W. Tian, "A model combining stacked auto encoder and back propagation algorithm for short-term wind power forecasting," *IEEE Access*, vol. 6, pp. 17851–17858, 2018.

[14] M. Javadi, A. M. Malyscheff, D. Wu, C. Kang, and J. N. Jiang, "An algorithm for practical power curve estimation of wind turbines," *CSEE J. Power Energy Syst.*, vol. 4, no. 1, pp. 93–102, Mar. 2018.

[15] M. Sharifzadeh, F. Separi, and M. Heydari, "Planning of autonomous smart micro grid for electrification of remote villages in MEDC," *CIRED-Open Access Proc. J.*, vol. 2017, no. 1, pp. 2493–2495, Oct. 2017.

[16] A. Kumar, B. Sah, Y. Deng, X. He, P. Kumar, and R. C. Bansal, "Application of multi-criteria decision analysis tool for design of a sustainable micro-grid for a remote village in the Himalayas," *J. Eng.*, vol. 2017, no. 13, pp. 2108–2113, 2017.

[17] S. Pachpor and H. M. Suryawanshi, "Design and analysis of triplen controlled resonant converter for renewable sources to interface DC micro grid," *IEEE Access*, vol. 7, pp. 15330–15339, 2019.

[18] A. Fathi, Q. Shafiee, and H. Bevrani, "Robust frequency control of microgrids using an extended virtual synchronous generator," *IEEE Trans. Power Syst.*, vol. 33, no. 6, pp. 6289–6297, Nov. 2018.

[19] J. Li, J. Fang, I. Wen, Y. Pan, and Q. Ding, "Optimal trade-off between regulation and wind curtailment in the economic dispatch problem," *CSEE J. Power Energy Syst.*, vol. 1, no. 4, pp. 37–45, Dec. 2015.

[20] A. Goudarzi, A. Ahmadi, A. G. Swanson, and J. Van Coller, "Non-convex optimisation of combined environmental economic dispatch through cultural algorithm with the consideration of the physical constraints of generating units and price penalty factors," *SAIEE Afr. Res. J.*, vol. 107, no. 3, pp. 146–166, Sep. 2016.

[21] Z. Yang, K. Li, Q. Niu, Y. Xue, and A. Foley, "A self-learning TLBO based dynamic economic/environmental dispatch considering multiple plug-in electric vehicle loads," *J. Mod. Power Syst. Clean Energy*, vol. 2, pp. 298–307, Dec. 2014, doi: 10.1007/s40565-014-0087-6.

[22] D. N. Jayakumar and P. Venkatesh, "Glowworm swarm optimization algorithm with topsis for solving multiple objective environmental economic dispatch problem," *Appl. Soft Comput.*, vol. 23, pp. 375–386, Oct. 2014.

[23] P. R. Ehrlich and P. H. Raven, "Butterflies and plants: A study in coevolution,"Evolution, vol. 18, no. 4, pp. 586–608, 1964.

[24] D. H. Janzen, "When is it coevolution?" *Evolution*, vol. 34, pp. 611–612, May 1980.

[25] S. Huang and V. Dinavahi, "Multi-group particle swarm optimisation for transmission expansion planning solution based on LU decomposition," *IET Gener., Transmiss. Distrib.*, vol. 11, no. 6, pp. 1434–1442, Apr. 2017.

[26] M. Hemmati, N. Amjady, and M. Ehsan, "System modeling and optimization for islanded micro-grid using multi-cross learning-based chaotic differential evolution algorithm," *Int. J. Electr. Power Energy Syst.*, vol. 56, no. 3, pp. 349–360, Mar. 2014.

[27] F. Zaman, S. M. Elsayed, T. Ray, and R. A. Sarker, "Co-evolutionary approach for strategic bidding in competitive electricity markets," *Appl. Soft Comput.*, vol. 51, pp. 1–22, Feb. 2017.

[28] Z. Ming, Q. Qiqi, W. Haojing, G. Yuming, G. Liang, Z. Jian, and Z. Huadong, "Economy benefit comparison of CCHP system and conventional separate supply system," in *Proc. 8th Int. Conf. Intell. Comput. Technol. Automat. (ICICTA)*, Nanchang, China, 2015, pp. 402–406.

[29] D. Li, W. Yan, W. Li, and Z. Ren, "A two-tier wind power time series model considering day-to-day weather transition and intraday wind power fluctuations," *IEEE Trans. Power Syst.*, vol. 31, no. 6, pp. 4330–4339, Nov. 2016.

[30] Y. Lin, M. Yang, C. Wan, J. Wang, and Y. Song, "A multi-model combination approach for probabilistic wind power forecasting," *IEEE Trans. Sustain. Energy*, vol. 10, no. 1, pp. 226–237, Jan. 2019.

[31] Q. Wang, C. B. Martinez-Anido, H. Wu, A. R. Florita, and B. Hodge, "Quantifying the economic and grid reliability impacts of improved wind power forecasting," in *Proc. IEEE Power Energy Soc. Gen. Meeting*, Chicago, IL, USA, Jul. 2017, p. 1.

[32] N. Huanna, Y. Lu, Z. Jingxiang, W. Yuzhu, W. Weizhou, and L. Fuchao, "Flexible-regulation resources planning for distribution networks with a high penetration of renewable energy," *IET Gener., Transmiss. Distrib.*, vol. 12, no. 18, pp. 4099–4107, Oct. 2018.

[33] J. Yan, F. Li, Y. Liu, and C. Gu, "Novel cost model for balancing wind power forecasting uncertainty," *IEEE Trans. Energy Convers.*, vol. 32, no. 1, pp. 318–329, Mar. 2017.

[34] M. Xie, S. Ke, J. Xiong, P. Cheng, and M. Liu, "Recursive dynamic regression-based two-stage compensation algorithm for dynamic economic dispatch considering high-dimensional correlation of multi-wind farms," *IET Renew. Power Gener.*, vol. 13, no. 3, pp. 475–481, Feb. 2019.

[35] M. Yin, Y. Xu, C. Shen, J. Liu, Z. Y. Dong, and Y. Zou, "Turbine stability-constrained available wind power of variable speed wind turbines for active power control," *IEEE Trans. Power Syst.*, vol. 32, no. 3, pp. 2487–2488, May 2017.

[36] P. Chen and T. Thiringer, "Analysis of energy curtailment and capacity overinstallation to maximize wind turbine profit considering electricity price–wind correlation," *IEEE Trans. Sustain. Energy*, vol. 8, no. 4, pp. 1406–1414, Oct. 2017.
[37] L. Jin and C. Zhang, "Process planning optimization with energy consumption reduction from a novel perspective: Mathematical modeling and a dynamic programming-like heuristic algorithm," *IEEE Access*, vol. 7, pp. 7381–7396, 2019.

BIFEI TAN received the B.E. degree in electrical engineering and automation from the South China University of Technology, China, in 2013 and 2017, respectively, where he is currently pursuing the Ph.D. degree in power system and its automation. His current research interests include economic dispatch in micro-grid, machine learning, energy transfer systems, and wind power forecasting.

HAOYONG CHEN (M'03–SM'10) received the B.S., M.S., and Ph.D. degrees in electrical engineering from Xi'an Jiaotong University, Xi'an, China, in 1995, 1997, and 2000, respectively. He is currently a Professor with the School of Electric Power, South China University of Technology, Guangzhou, China. He is also the Chair of Asia-Pacific Research Institute of Smart Grid and Renewable Energy, Hong Kong. His current research interests include power system operation/control, smart grids, computational intelligence applications, and power markets.